

Two-dimensional scalar spectra in the deeper layers of a dense and uniform model canopy

D. Poggi · G.G. Katul

Received: 29 August 2005 / Accepted: 20 March 2006 /
Published online: 3 June 2006
© Springer Science+Business Media B.V. 2006

Abstract The turbulent flow inside dense canopies is characterized by wake production and short-circuiting of the energy cascade. How these processes affect passive scalar concentration variability in general and their spectral properties in particular remains a vexing problem. Progress on this problem is frustrated by the shortage of high resolution spatial concentration measurements, and by the lack of simplified analytical models that connect spectral modulations in the turbulent kinetic energy (TKE) cascade to scalar spectra. Here, we report the first planar two-dimensional scalar concentration spectra (ϕ_{cc}) inside tall canopies derived from flow visualization experiments. These experiments were conducted within the deeper layers of a model canopy composed of densely arrayed cylinders welded to the bottom of a large recirculating water channel. We found that in the spectral region experiencing wake production, the ϕ_{cc} exhibits directional scaling power laws. In the longitudinal direction (x), or the direction experiencing the largest drag force, the $\phi_{cc}(k_x)$ was steeper than $k_x^{-5/3}$ and followed an approximate $k_x^{-7/3}$ at wavenumbers larger than the injection scale of wake energy, where k_x is the longitudinal wavenumber. In the lateral direction (y), the spectra scaled as $k_y^{-5/3}$ up to the injection scale, and then decayed at an approximate $k_y^{-7/3}$ power law. This departure from the classical inertial subrange scaling (i.e., $k^{-5/3}$) was reproduced using a newly proposed analytical solution to a simplified scalar spectral budget equation. Near the velocity viscous dissipation range, the scalar spectra appear to approach an approximate k^{-3} , a tantalizing result consistent with dimensional analysis used in the inertial-diffusive range. Implications to subgrid modelling for large-eddy simulations (LES) inside canopies are briefly discussed.

D. Poggi

Dipartimento di Idraulica, Trasporti ed Infrastrutture Civili, Politecnico di Torino, Torino, Italy
Nicholas School of the Environment and Earth Sciences, Duke University, Durham, NC, USA
Department of Civil and Environmental Engineering, Duke University, Durham, NC, USA

G. G. Katul (✉)

Nicholas School of the Environment and Earth Sciences, Duke University, Durham, NC, USA
Department of Civil and Environmental Engineering, Duke University, Durham, NC, USA
E-mail: gaby@duke.edu

Keywords Canopy turbulence · Laser-induced fluorescence technique · Two-dimensional scalar spectra · Wake production

1 List of symbols

| Symbol | Definition |
|-----------------|--------------------------------------------------------------------------------------------------------------------------------------|
| a | Leaf area density or frontal area index |
| B_{cc} | Spatial covariance of the turbulent concentration = $\overline{c(x_j)c(x_j + r_j)}$ |
| B_{jcc} | = $\overline{u_j(x_j)c(x_j)c(x_j + r_j)}$ |
| $c(x_j, t)$ | Scalar concentration at time t and position x_j |
| C_d | Drag coefficient |
| C_o | The Kolmogorov constant for the energy spectrum (= 0.5) |
| d_r | The rod diameter |
| e | Turbulent kinetic energy (or TKE) |
| h | The canopy height |
| h_w | The boundary-layer height (or depth of water in the flume) |
| k_x, k_y, k | Longitudinal, lateral, and total wavenumbers, respectively |
| L_r | The longitudinal rod spacing |
| N_* | Scalar variance dissipation rate |
| r_j | Separation distance between two points along direction x_j |
| t | Time |
| u_j | Longitudinal ($j = 1$), lateral ($j = 2$), and vertical ($j = 3$) turbulent velocities |
| $W_c(t, k)$ | Transfer of scalar energy across wavenumber k at time t |
| x_j | Longitudinal (x) direction when $j = 1$, lateral (y) and vertical (z) direction when $j = 2$ and $j = 3$, respectively |
| χ_c | Molecular diffusivity of scalar c |
| δ | Scalar similarity constant (= 0.63) |
| ϵ | Turbulent kinetic energy dissipation rate |
| ν_t | Turbulent viscosity |
| ϕ_{cc} | Spatial energy spectrum of the concentration |
| ϕ_{ee} | Energy spectrum of the turbulent kinetic energy |
| ϕ_{uu} | Energy spectrum of the longitudinal velocity |
| $\sigma_c^2(t)$ | Spatial variance of the concentration at time t |

2 Introduction

Studies on scalar concentration (c) variability in a turbulent flow inside roughness elements are now receiving significant attention in many engineering and geoscience fields including atmospheric chemistry and pollution exposure, odour distribution and chemotactic algorithms in biological systems, contaminant dispersion inside urban areas, and biosphere-atmosphere CO₂ exchange near the soil surface inside tall canopies, to name a few (see Katul and Albertson 1999; Shraiman and Siggia 2000; Warhaft 2000; Finnigan 2000; Siqueira et al. 2002; and Cheng and Castro 2002). The turbulent scales contributing to the variance in c are often examined using spectral (or structure function) analysis because such analysis can identify universal scaling laws or active eddy sizes responsible for the large c excursions.

In the roughness sublayer above uniform canopies, the turbulent eddy motion is known to exhibit three spectral regions: (1) The energy containing range (or large-scale turbulence), in which turbulent kinetic energy (TKE) per unit mass is produced, (2) the inertial subrange (hereafter referred to as ISR), in which TKE is neither produced nor dissipated, but is simply transported from large to small scales, and (3) the dissipation range, where TKE is converted to internal energy by the action of fluid viscosity (Fig. 1).

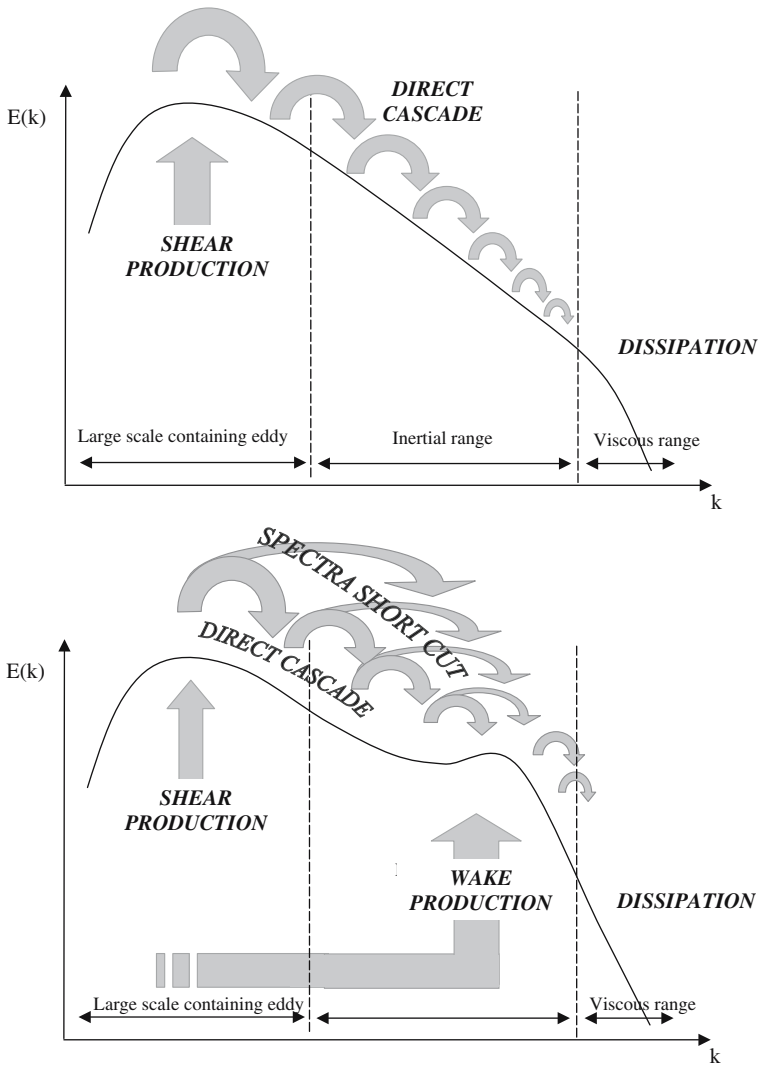


Fig. 1 Schematic diagram of the TKE spectrum showing the three spectral regions above the canopy (*top*) and how the canopy elements modify this spectrum by wake production and short-circuiting of the energy cascade (*bottom*; revised from Kaimal and Finnigan, 1994)

Inside roughness elements, two additional processes impact the TKE spectral properties: (1) the work that the mean flow exercises against the foliage drag thereby producing TKE by wakes (hereafter referred to as WKE), and (2) the spectral short-circuiting of the energy cascade that represents the same physical process but is acting on turbulent eddies rather than on the mean flow (Wilson 1988; Kaimal and Finnigan 1994; Finnigan 2000). These two processes are known to impact a broad range of scales. Scales larger than the canopy elements can gain some TKE because of WKE but can lose TKE because of the short-circuiting of the energy cascade (Fig. 1). Scales smaller than the canopy elements can gain TKE from both the WKE and the short-circuiting of the energy cascade. All these effects

alter the classical TKE cascade thereby violating assumptions used to derive the spectral properties of velocity and scalars within the ISR (Fig. 1). While this spectral picture received some field experimental support (Finnigan 2000), and was shown to be reasonable for a wide range of canopy roughness densities for velocities (Poggi et al. 2004c), little is known about how these two processes modulate the spectra of passive scalars, the subject of this study. This knowledge gap may well be attributed to the lack of detailed high resolution spatio-temporal concentration data, and perhaps due to the absence of simplified phenomenological theories that analytically link the canopy attributes to departures from ISR scaling.

The main objective here is to investigate how wake production and short-circuiting of the energy cascade (shown schematically in Fig. 1) impact the two-dimensional (planar) spectra of passive scalars inside a model canopy. In particular, we seek to understand how wake production modifies the ISR scaling laws using measured 2-D scalar spectra, and whether simplified analytical models based on spectral budgets can theoretically predict them. To achieve the study objective, detailed flume experiments were conducted in which scalar concentration fluctuations were sampled at high spatial and temporal resolution in the lower layers of a dense uniform canopy composed of rods. We emphasize that other processes such as unsteadiness in the mean flow conditions, density gradients, variability in canopy morphology, and complex scalar source-sink distributions inside the canopy can impact the scalar concentration spectra; however, exploring all of them simultaneously is well beyond the scope of a single study.

3 Experiments

Much of the experimental set-up is described elsewhere (Poggi et al. 2006); however, a review of the salient features relevant to this analysis is presented here. The experiment was conducted at the Giorgio Bidone hydraulics laboratory, DITIC Politecnico di Torino, in a recirculating constant head rectangular flume, 18 m long, 0.90 m wide, and 1 m deep. The walls are made of clear glass to permit optical access. The canopy is placed in a test section 9 m long and 0.9 m wide situated about 7 m downstream from the channel entrance. The canopy is composed of vertical cylinders, 120 mm tall ($= h$) and 4 mm in diameter ($= d_r$) arrayed in a regular pattern at a density of 1072 rods m^{-2} . Such a density is equivalent to a dense canopy having an element area index (frontal area per unit volume) of $4.27 m^2 m^{-3}$. The measured drag coefficient (C_d) is comparable to drag coefficients already reported for dense forested ecosystems with leaf area index (LAI) ranging from 3.5 to 6.0 (Katul and Chang 1999; Katul et al. 2004; Poggi et al. 2004a). The velocity and scalar concentration measurements were conducted when the water depth ($= h_w$) attained a constant value of 0.6 m.

The longitudinal (u_1) and vertical (u_3) velocity time series were measured by a two-component laser Doppler anemometry (LDA) at various points within and above the canopy (see Poggi et al. 2004c). The advantages of the LDA over other techniques for measuring velocity fluctuations near obstacles are discussed elsewhere (Poggi et al., 2002). Here, we focus on measurements conducted at $z/h = 1/6$ and $z/h = 1/2$. These measurement depths were chosen because they bound the canopy region in which WKE is the largest term balancing the TKE mean dissipation rate (Poggi et al. 2004a; their Fig. 6), while the shear production of TKE remains the smallest term in the TKE budget. Hence, being the largest external energy source, we expect that WKE plays a significant role in this region in terms of its impact on scalar concentration variability (see also Poggi et al. 2004d). The spectra in these two planes will also be contrasted with measured spectra collected at $z/h = 2$. The

latter spectra are not influenced by any WKE and serve as a logical reference for quantifying the effects of the canopy on the energy cascade schematically postulated in Fig. 1.

The LDA planar location within the rods was chosen such that the measured local temporal statistics were representative of the horizontally averaged temporal statistics, following an analysis of the more spatially expansive data for the model canopy discussed elsewhere (Poggi et al. 2004a, b, c). The sampling duration and frequency were 3600 s per run at 2500 – 3000 Hz. The experiment was conducted at two bulk Reynolds numbers, $Re_b = 116, 560$ and $Re_b = 172, 300$, to assess the robustness of the spectral scaling laws for velocity and scalar concentration to variations in Re_b (for large Re_b). The Re_b was calculated using the vertically-averaged velocity (U_b) across h_w as a characteristic velocity, with h_w as a characteristic length scale.

The laser-induced fluorescence (LIF) technique was used to measure the local instantaneous dye concentration in a plane parallel to the channel bottom. The measurements were conducted by injecting Rhodamine 6G in a manner to resemble a line source. A lens system was used to provide a 0.6 mm thick light sheet of about 120 mm in width and 40 mm in length (Fig. 2). Image sequences were recorded for an area in the horizontal plane centered in the middle of the channel using a colour CCD video camera. This video set-up allowed us to acquire digital movies with high resolution (704 x 576 pixels corresponding to a resolution of 0.17 mm, DV-AVI with PAL format and high frequency of 25 frames per second). A 6-min video sequence was used to compute the instantaneous 2-D planar concentration. Four video sequences were acquired corresponding to two depths ($z/h = 1/6$ and $z/h = 1/2$) and two bulk Reynolds numbers ($Re_b = 116, 560$ and $Re_b = 172, 300$). Images from these four videos were then used to compute the 2-D scalar spectra and test simplified models derived from an integrated spectral budget.

4 Theory

In the absence of local sources and sinks, the continuity equation for a passive scalar c at time t and a point x_j is given by

$$\frac{\partial c}{\partial t} + \frac{\partial u_j c}{\partial x_j} = \chi_c \frac{\partial^2 c}{\partial x_j x_j} \quad (1)$$

where x_j ($x_1 = x$, $x_2 = y$, $x_3 = z$) are the longitudinal, lateral, and vertical directions, respectively; u_j ($u_1 = u$, $u_2 = v$, $u_3 = w$) are the instantaneous velocity components along x_j , and χ_c is the molecular diffusivity of the passive scalar. Formally, a passive scalar is defined as a contaminant in a moving fluid stream that is present in such low concentrations that it has no dynamical effect on the motion itself.

4.1 The spectral budget

If \hat{c} represents the concentration at another point \hat{x}_j , separated by a distance $|r|$ from x_j , then the instantaneous covariance equation is given by

$$\frac{\partial c \hat{c}}{\partial t} + \frac{\partial u_j c \hat{c}}{\partial x_j} + \frac{\partial \hat{u}_j c \hat{c}}{\partial \hat{x}_j} = \chi_c \frac{\partial^2 c \hat{c}}{\partial x_j x_j} + \chi_c \frac{\partial^2 c \hat{c}}{\partial \hat{x}_j \hat{x}_j}, \quad (2)$$

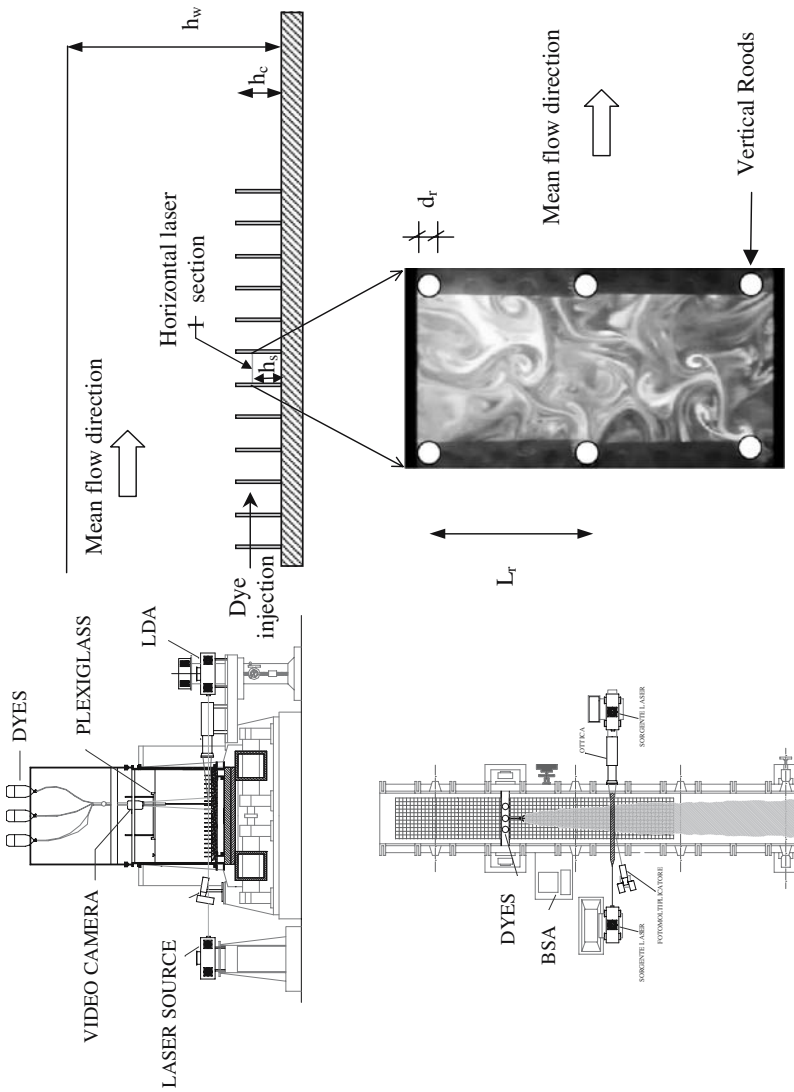


Fig. 2 Experimental set-up of the scalar dispersion experiment. *Bottom-left* is a schematic of the lateral section view showing the location of the LIF source and the video camera; *top-left* is a longitudinal section view showing the dye release in relation to the model canopy; *bottom-right* is a plan view showing the source position and the 2-D area sampled by the camera in relation to the source; *top-right* is a sample image at one instant in time of the 2-D relative scalar concentration field showing the generation of von-Karman streets. The rod diameter (d_r) and rod spacing are also shown for reference

where $r = [(x_1 - \hat{x}_1)^2 + (x_2 - \hat{x}_2)^2 + (x_3 - \hat{x}_3)^2]^{1/2}$. Upon defining the spatial covariance function $B_{cc}(t, r) = \overline{c \hat{c}}$ and averaging Eq. 2, we obtain:

$$\frac{\partial B_{cc}}{\partial t} - 2 \frac{\partial B_{jcc}}{\partial r_j} = 2\chi_c \frac{\partial^2 B_{cc}}{\partial r^2}, \tag{3}$$

where the overline indicates spatial averaging, $B_{jcc} = \overline{u_j(x_j)c(x_j)c(x_j + r_j)}$, and $r_j = \hat{x}_j - x_j$. The energy spectrum of $c = \phi_{cc}(t, k)$ is related to $B_{cc}(t, r)$ via

$$\phi_{cc}(t, k) = \frac{2}{\pi} \int_0^\infty B_{cc}(t, r)kr \sin(kr)dr. \tag{4}$$

Note that $\int_0^\infty \phi_{cc}(t, p)dp = \sigma_c^2(t)$ is the concentration spatial variance, and k is the spherical wavenumber ($= (k_x^2 + k_y^2 + k_z^2)^{1/2}$).

Upon multiplying Eq. 3 by $(2/\pi)kr \sin(kr)$ and integrating across all k yields

$$\frac{\partial \phi_{cc}(t, k)}{\partial t} = W_c(t, k) - 2\chi_c k^2 \phi_{cc}(t, k), \tag{5}$$

where $W_c(t, k)$ represents the transfer of scalar energy via interactions between turbulent velocity and scalar concentration fluctuations. If no scalar energy is lost or gained while being transferred, then $W_c(t, k)$ must necessarily satisfy the integral condition

$$\int_0^\infty W_c(t, p)dp = 0. \tag{6}$$

The scalar variance dissipation rate $N_*(t)$ is linked to the molecular dissipation term via

$$N_*(t) = \chi_c \int_0^\infty p^2 \phi_{cc}(t, p)dp. \tag{7}$$

Defining $F_c(t, k) = \int_0^k W_c(t, p)dp$, and noting that for sufficiently large k (say comparable ISR scales if any) we can assume that

$$\frac{\partial}{\partial t} \int_k^\infty \phi_{cc}(t, p)dp \ll \frac{\partial}{\partial t} \int_0^\infty \phi_{cc}(t, p)dp \tag{8}$$

so that

$$-N_*(t) = \frac{\partial}{\partial t} \int_0^\infty \phi_{cc}(t, p)dp \simeq \frac{\partial}{\partial t} \int_0^k \phi_{cc}(t, p)dp, \tag{9}$$

and upon integrating Eq. 5, we obtain the well-known ‘integrated spectral budget’ (Panchev 1971; Monin and Yaglom 1975; Lesieur 1991),

$$N_*(t) = F_c(t, k) + 2\chi_c \int_0^k p^2 \phi_{cc}(t, p)dp. \tag{10}$$

To solve for $\phi_{cc}(t, k)$, closure models for $F_c(t, k)$ must be developed that take advantage of the spectral properties of the velocity (or TKE).

4.2 Closure models

The simplest first-order spectral closure model for $F_c(t, k)$ is a local eddy-diffusivity $\chi_t(t, k)$ (i.e., turbulent dissipation resembling molecular dissipation), resulting in

$$F_c(t, k) = 2\chi_t(t, k) \int_0^k p^2 \phi_{cc}(t, p)dp, \tag{11}$$

where $\chi_t(t, k)$ is the local spectral eddy diffusivity. With such a closure, Eq. 10 becomes

$$\frac{N_*(t)}{\chi_t(t, k) + \chi_c} = 2 \int_0^k p^2 \phi_{cc}(t, p) dp, \tag{12}$$

and whose solution is given by

$$\phi_{cc}(t, k) = -\frac{1}{2} \left(\frac{N_*(t)}{(\chi_t(t, k) + \chi_c)^2} \right) \frac{d\chi_t(t, k)}{dk} k^{-2}. \tag{13}$$

To compute $\phi_{cc}(t, k)$, it is necessary to model $\chi_t(t, k)$ from the TKE given that the latter quantity is primarily affected by wake production. The simplest model is $\chi_t(t, k) = \delta v_t(t, k)$, where δ is a proportionality constant that will be determined later, and v_t is the turbulent eddy viscosity responsible for the TKE transfer.

From the TKE spectral budget (see Panchev 1971; Tennekes and Lumley 1972),

$$v_t(t, k) = \frac{\epsilon(t)}{\int_0^k 2p^2 \phi_{ee}(t, p) dp}, \tag{14}$$

where $\epsilon(t)$ is the TKE dissipation rate and ϕ_{ee} is the spectrum of the TKE with TKE defined as $e = (1/2)(u_1^2 + u_2^2 + u_3^2)$. Hence, if the canopy WKE effects on $\phi_{ee}(k)$ can be modelled, the eddy viscosity and $\phi_{cc}(k)$ can then be readily computed. Note that if $\phi_{ee}(k) \sim k^{-\alpha}$, then $\phi_{cc}(k) \sim k^{-\alpha}$.

4.3 Drag effects on $\phi_{ee}(k)$

In the absence of any canopy drag, and after sufficient cascading steps, the classical Kolmogorov spectrum (Kolmogorov 1941) within the ISR yields

$$\phi_{ee}(k) = C_o \epsilon^{2/3} k^{-5/3}, \tag{15}$$

where $C_o = 0.5$ is the Kolmogorov constant (hereafter, we refer to this spectrum as *K41*). Furthermore, the derivation of *K41* requires that such scaling holds along k_x , k_y , and k_z by virtue of local isotropy.

In the presence of canopy drag in direction x_1 , the ISR cascade is short-circuited by wake production. Finnigan (2000) argued that the loss of energy from waveband k_1 and $k_1 + dk_1$ is given by

$$\frac{dS}{dk_1} = -\frac{3}{2} C_d a \overline{u_1} \phi_{uu}(k_1), \tag{16}$$

where C_d is the drag coefficient that can vary with the mean velocity (Poggi et al. 2004a,c), ϕ_{uu} is the velocity spectrum of u_1 , and a is the local leaf area density. Finnigan (2000) further argued that this loss can be expressed as $S(k) = \sigma(k) \phi_{uu}(k)$, where σ is the rate at

which an energy spectral element is transferred across k . If $\epsilon/(d\epsilon/dk) \ll 1$, then the TKE dissipation rate is not significantly altered from its ISR value, and (heuristic) dimensional arguments result in $\sigma(k) = C_o^{-1} \epsilon^{1/3} k^{5/3}$. This assumption about the TKE dissipation is also implicit in the derivation of the eddy-viscosity model in Eq. 14 as discussed in Katul and Chu (1998). Upon replacing this phenomenological model for $S(k)$ into Eq. 16, we obtain a first-order ordinary differential Equation for $\phi_{uu}(k)$ given by

$$\frac{d}{dk_1} (C_o^{-1} \epsilon^{1/3} k_1^{5/3} \phi_{uu}(k_1)) = -\frac{3}{2} C_d a \bar{u}_1 \phi_{uu}(k_1), \tag{17}$$

whose solution is

$$\phi_{uu}(k_1) = a_1 k_1^{-5/3} \exp(a_2 k_1^{-2/3}), \tag{18}$$

where $a_1 = C_o \epsilon^{1/3}$ and $a_2 = \frac{4}{9} C_d a \bar{u}_1 \epsilon^{-1/3}$. Hereafter, this spectrum is referred to as the Finnigan spectrum.

4.4 Linearized spectral models for passive scalars within the wake production region

To track the ‘first-order’ effects of the wake production region on the scalar spectrum in the Finnigan model, we consider a Taylor series expansion of

$$\exp(a_2 k_1^{-2/3}) = 1 + a_2 k_1^{-2/3} + \dots \tag{19}$$

and retain the two leading order terms so that

$$\phi_{uu}(k_1) \sim a_1 k_1^{-5/3} (1 + a_2 k_1^{-2/3}). \tag{20}$$

Furthermore, if ϕ_{ee} scales as ϕ_{uu} , then the resulting eddy viscosity is given by

$$\nu_t(k_1) = \frac{3\epsilon}{2a_1(a_2 + k_1^{2/3})k_1^{2/3}}, \tag{21}$$

and the resulting scalar spectrum for this eddy diffusivity ($= \delta \nu_t$), assumed to be much larger than χ_c , is given by

$$\phi_{cc}(k_1) = \frac{2}{9\delta} a_1 \frac{N_*}{\epsilon} (a_2 + 2k_1^{2/3}) k_1^{-7/3}. \tag{22}$$

Two asymptotic power laws emerge from this linearized spectrum: the first is when $C_d \rightarrow 0$, the spectrum reduces (as expected) to its familiar *K41* form in the ISR, given by

$$\phi_{cc}(k_1) = \frac{C_o}{\delta} \epsilon^{-2/3} N_* k_1^{-5/3}. \tag{23}$$

The second is when $a_2 \gg k^{2/3}$ and the scalar spectrum reduces to

$$\phi_{cc}(k_1) = \frac{C_o}{\delta} \epsilon^{-2/3} N_* \left[\frac{4}{3} C_d a \bar{u}_1 \epsilon^{-1/3} \right] k_1^{-7/3}. \tag{24}$$

This analysis suggests that power laws of scalar spectra most affected by the drag force are steeper than $-5/3$ and are likely to scale (in the limit) as $-7/3$. Note that for these two asymptotic cases, ϕ_{uu} follows the same power laws as ϕ_{cc} .

From the ISR limit, the similarity constant δ can be determined by noting that the Kolmogorov constant for scalars is $(C_o/\delta) = 0.8$ resulting in $\delta = 0.63$ (see discussion in Hsieh and Katul 1997). With this estimate of δ , all the constants are known.

In short, the combination of Eqs. 13, 18, the linear expansion in Eq. 19, the eddy-viscosity model in Eq. 21, and the scalar spectrum in Eq. 22 represent the main novelties of this derivation. Whether the asymptotic scaling laws derived in Eqs. (23) and (24) are robust to all these assumptions and simplifications are considered next within the context of the LDA and LIF measurements.

5 Results

The LDA-measured u and w time series were used to compute $\phi_{uu}(k_x)$ and $\phi_{ww}(k_x)$ shown in Fig. 3 for $Re_b = 172, 300$, where k_x is determined from the mean longitudinal velocity using Taylor's frozen turbulence hypothesis. For $z/h = 1/6$, the LDA-measured $\phi_{uu}(k_x)$ is clearly affected by wake production, which occurs on scales larger than d_r but smaller than the rod spacing (L_r). In fact, measured $\phi_{uu}(k_x)$ and $\phi_{ww}(k_x)$ both suggest that the WKE energy is injected at scales comparable to $5d_r$. This is not surprising given that $d_r/0.21 (= 4.8d_r)$ can be derived from the Strouhal number that links the frequency of the von Karman streets vortical motion to the characteristic length scale of the obstacle (d_r). A cautionary note here is that in 'real canopies', this WKE injection scale may be 'masked' because of the multiplicity of obstacle diameters. Following the wake production wavenumbers, $\phi_{uu}(k_x)$ exhibits a $k_x^{-7/3}$ with increasing k_x consistent with the second asymptotic limit of the linearized model. For $\phi_{ww}(k_x)$, a direction less affected by the drag force, an approximate $k_x^{-5/3}$ scaling persists with increasing k_x immediately following the wake energy injection wavenumber.

For $z/h = 1/2$, the measured $\phi_{uu}(k_x)$ remains affected by WKE, and the $k_x^{-7/3}$ scaling persists with increasing k_x following the wake production. However, the wavenumber range is not as extensive as its $z/h = 1/6$ counterpart. For $\phi_{ww}(k_x)$, the impact of the wake production appears 'smeared' in wavenumber space and hence the energy content of the WKE appears 'broadened' over a wider range of k_x . An approximate $k_x^{-5/3}$ scaling follows the WKE injection with increasing k_x .

Above the canopy ($z/h = 2$), the standard ISR scaling clearly holds in both ϕ_{uu} and ϕ_{ww} . In fact, the contrast in the spectra measured at $z/h = 1/6$ and $z/h = 2$ almost mirrors the conceptual spectra shown in Fig. 1. We repeated the same analysis for the lower Re_b case and found that these spectral results are not significantly changed (not shown).

Figure 4 shows the ensemble 2-D spectra $\phi_{cc}(k_x)$, $\phi_{cc}(k_y)$ for both Re_b and both z/h . The ensemble averaging was conducted on all 9,000 ($= 6 \text{ min} \times 60 \text{ s min}^{-1} \times 25 \text{ images s}^{-1}$) images. For $\phi_{cc}(k_x)$, an approximate $-7/3$ power law emerges with increasing k_x from the data immediately following the WKE injection wavenumber, consistent with $\phi_{uu}(k_x)$. This scaling appears robust to variations in z/h and Re_b (at least within the range of the experiment), and is consistent with the linearized model predictions. For $\phi_{cc}(k_y)$ and with increasing k_y , an approximate $k_y^{-5/3}$ scaling exists for scales between the rod spacing and the injection wavenumbers, followed by a transition region, and then a rather limited $k_y^{-7/3}$ scaling up to $kd_r = 2$. Again, these scaling laws appear to persist for both Re_b and z/h runs. Recall that the von Karman streets are highly anisotropic and are much more elongated along k_x than k_y . This is the primary reason why the $-7/3$ power law is much more extensive along the primary drag-force direction.

A tantalizing result in Fig. 4 is that ϕ_{cc} appears to be consistent with a k^{-3} scaling for $kd_r > 5$, which is more evident in the higher Re_b runs. This wavenumber limit and scaling

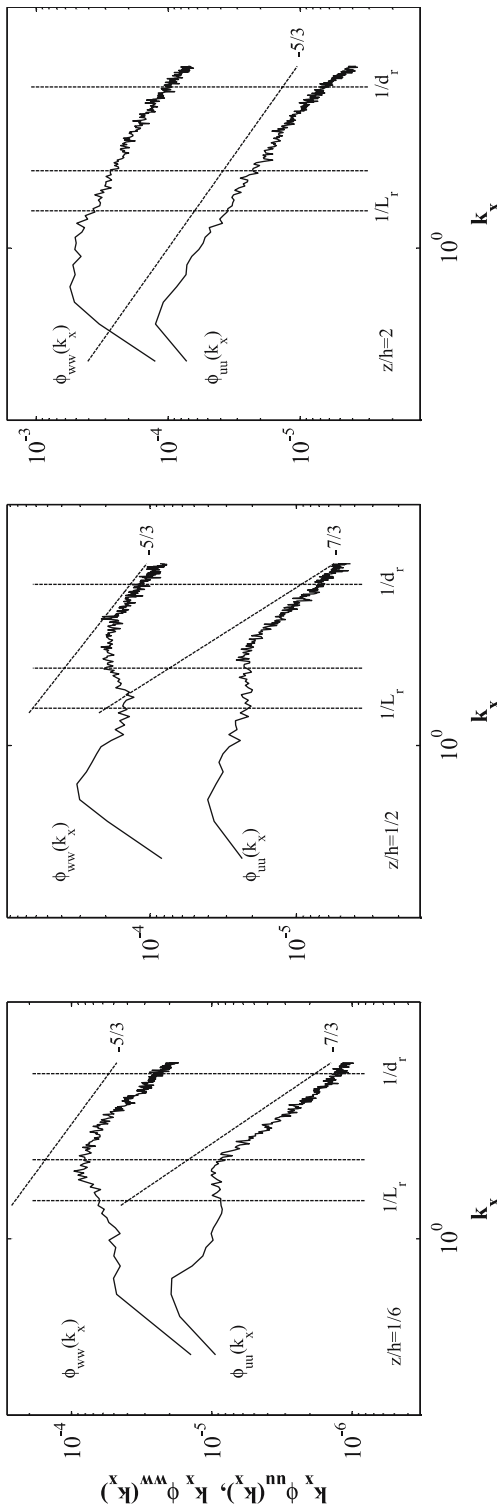


Fig. 3 The measured longitudinal (ϕ_{uu}) and vertical (ϕ_{ww}) velocity spectra (shown as $k_x \phi(k_x)$) as a function of the longitudinal wavenumber k_x (determined from Taylor's frozen turbulence hypothesis) at $z/h = 1/6$ (left), $1/2$ (middle), and 2.0 (right). The $-5/3$ and $-7/3$ equivalent scaling laws are also shown for reference in the left and middle panels. For the right panel, only the $-5/3$ power law is shown as drag effects are not relevant at $z/h = 2$. The wavenumbers corresponding to the rod spacing ($1/L_r$) and rod diameter ($1/d_r$) are shown as vertical lines, while the WKE injection scale, determined from the Strouhal number (i.e., the wavenumber corresponding to $4.8d_r$), is also shown

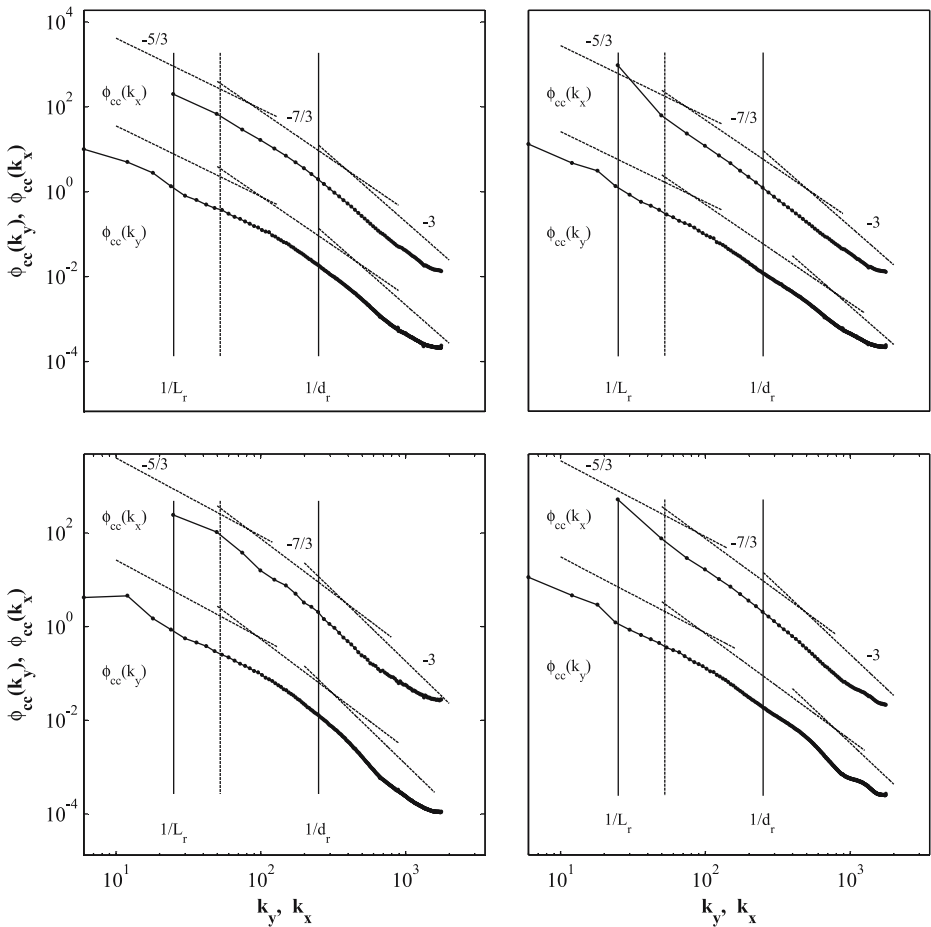


Fig. 4 The ensemble-averaged (in time) of the measured scalar spectra (ϕ_{cc}) along the longitudinal (k_x) and lateral (k_y) wavenumber directions at $z/h = 1/6$ (top), $1/2$ (bottom) for $Re_b = 116, 560$ (left) and $Re_b = 172, 300$ (right). The $\phi_{cc}(k_x)$ is displaced by 2 decades above the $\phi_{cc}(k_y)$. The $-5/3$, the $-7/3$, scaling laws are also shown for reference. Also, the Gibson -3 power law derived for the inertial-diffusive range is presented for the very large wavenumbers. The wavenumbers corresponding to the rod spacing ($1/L_r$) and rod diameter ($1/d_r$) are shown as vertical solid lines, while the WKE injection scale is shown as a dashed vertical line

law cannot be rigorously verified with just under $1/3$ of a decade of concentration measurements here, superimposed on potential measurement noise. Possible arguments leading to the emergence of a -3 power law in this wavenumber range have already been proposed by Gibson (1968) for the inertial-diffusive range (see Majda and Kramer 1999 for a rigorous argument). Gibson’s argument can be distilled to the following: if the variables affecting ϕ_{cc} are N_* , k , and χ , then dimensional analysis leads to

$$\phi_{cc}(k) = C_2 \frac{N_*}{\chi} k^{-3}, \tag{25}$$

where C_2 is a similarity constant. In such a dimensional analysis, any ‘scale-independent’ diffusivity can substitute for χ , though at such high wavenumbers, molecular diffusivity is

likely to exceed $\chi_t(k)$ and remains the logical choice. An alternative to the Gibson spectrum for canopy turbulence may be the Batchelor spectrum for the viscous-convective range (see Majda and Kramer 1999). Here, if the variables affecting ϕ_{cc} are N_* , k , and the maximum strain rate (S_r), then dimensional analysis leads to

$$\phi_{cc}(k) = C_3 N_* S_r k^{-1}, \quad (26)$$

where C_3 is a similarity constant. Again, any scale-independent strain rate can be used in this dimensional analysis (e.g., $\overline{u_1}/d_r$). It is clear that the ϕ_{cc} data in Fig. 4 remain steeper than k^{-1} for $kd_r > 5$ and appear not to contradict the Gibson spectrum results.

Finally, recall that Eq. 22 is the sum of two power laws and both can contribute to various wavenumber ranges; hence, precise power laws are not what the linearized model predicts except for the two asymptotic limits. We focused on these two asymptotic power-laws in Fig. 4 because (1) they facilitate comparisons and assist in identifying regime shifts in the spectral budget physics (e.g., from ISR to WKE dominated regime), and (2) power-law results are more transferable and their comparisons do not require a priori computations of $\epsilon(t)$, $N_*(t)$, and local $C_d(t, u_1)$ (image by image). The latter variables are difficult to determine.

6 Discussion and conclusions

While unsteadiness in the mean flow conditions, density gradients, variability in canopy morphology, and complex source-sink distributions are known to affect turbulent scalar spectra in real canopies, the defining syndrome of flows inside roughness elements remains the short-circuiting of the energy cascade through wake production. This is also the mechanism that is most difficult to resolve in field experiments because of the large effort needed to set up a spatial array of concentration measurements, and because the commonly used sonic anemometers measuring velocity statistics cannot sample the WKE injection scale. Here, we focused on how wake production and short-circuiting of the energy cascade affect the two-dimensional (planar) spectra of passive scalars inside a model canopy composed of densely arrayed cylinders for stationary flows, uniform canopy, with a well-defined scalar source location and injection rate. Even within this restricted scope, we showed that the scalar spectral budget equation remains complicated by numerous factors related to the transfer of scalar energy from the velocity field. Notwithstanding these complications, analytical model results were derived for idealized cases that successfully explained the spectral exponents (particularly the $-5/3$ and $-7/3$) and the anisotropy in those exponents observed in the scalar experiments (Fig. 4). However, because we do not have the spatial velocity statistics (e.g., the spatially averaged TKE and its dissipation at every instant in time), and because the LIF measures relative concentration and not absolute concentration, it is not possible to test these model predictions beyond power-law regimes.

Despite this agreement between theory and experiments for the power laws, several difficult issues, listed below, plagued the proposed model derivation:

- (1) The domain is assumed unbounded in all three Cartesian directions (e.g., $k \in [0, \infty)$), which is clearly unrealistic for these flume experiments. This assumption becomes less critical if the energy transfer function $F_c(t, k)$ is dominated by local interactions in wavenumber space. Likewise, the use of an eddy-viscosity model a priori assumes local wavenumber interactions.
- (2) The energy loss due to drag is not sufficiently large so that $\frac{\epsilon}{d\epsilon/dk} \ll 1$. This assumption was used in the derivation of ν_t and the Finnigan spectrum, and is unrealistic globally

across all wavenumber ranges. For the range of wavenumbers considered here (i.e., from rod spacing to rod diameter), and for the purposes of computing departures from ISR scaling, this assumption may be reasonable.

- (3) The Finnigan spectrum is used as a model for ϕ_{ee} along with all its simplifications and semi-empirical assumptions, and the retention of only two terms in the Taylor series expansion minimally needed to quantify the drag contribution effects on ϕ_{ee} . This is perhaps the most restrictive step in the entire derivation. Some support for the Finnigan spectrum was already provided from the LDA data in Fig. 3, though caution must be exercised about generalizations given the use of Taylor's frozen turbulence hypothesis in computing k_x .

Lastly, we envision the broader impact of this work to be two-fold:

- (1) *Experimental*: the 2-D measured scalar concentration spectra reported here can serve as benchmark for testing future subgrid models in large-eddy simulations (LES) of scalar transfer. The LES spatial grid resolution inside canopies rarely resolves the canopy spacing, and never resolves the rod diameter. In dense canopies, we showed that these two scales bound the wavenumber region experiencing much of the WKE production and ISR modulation. The latter is rarely considered in canopy LES.
- (2) *Theoretical*: the proposed analysis here is among the first to successfully show how scalar concentration spectra are modulated by wake production inside canopies using a simplified eddy-viscosity approach. The eddy viscosity model proposed in Eq. 21 can serve as a logical starting point to replace the classical Smagorinsky type models (e.g., Smagorinski 1993) with ones that are capable of explicitly accounting for canopy drag effects.

Acknowledgements The authors acknowledge the support of the National Science Foundation (NSF-EAR and NSF-DMS), the Biological and Environmental Research (BER) Program of the US Department of Energy, through the Southeast Regional Center (SERC) of the National Institute for Global Environmental Change (NIGEC), and through the Terrestrial Carbon Processes Program (TCP) and the FACE-FACTS project.

References

- Cheng H, Castro I (2002) Near wall flow over urban-like roughness. *Boundary-Layer Meteorol* 104:229–259
- Finnigan J (2000) Turbulence in plant canopies. *Ann Rev Fluid Mech* 32:519–571
- Gibson C (1968) Fine structure of scalar fields mixed by turbulence. II, Spectral Theory. *Phys Fluids* 11:2316–2327
- Hsieh C, Katul G (1997) The dissipation methods, Taylor's hypothesis, and stability correction functions in the atmospheric surface layer. *J Geophys Res* 102:16391–16405
- Kaimal J, Finnigan J (1994) *Atmospheric boundary layer flows: their structure and measurement*. Oxford University Press, New York, 289 pp
- Katul G, Albertson J (1999) Modeling CO₂ sources, sinks, and fluxes within a forest canopy. *J Geophys Res* 104:6081–6091
- Katul G, Chang W (1999) Principal length scales in second-order closure models for canopy turbulence. *J Appl Meteorol* 38:1631–1643
- Katul G, Chu C (1998) A theoretical and experimental investigation of the energy-containing scales in the dynamic sublayer of boundary-layer flows. *Boundary-Layer Meteorol* 86:279–312
- Katul G, Mahrt L, Poggi D, Sanz C (2004) One and two equation models for canopy turbulence. *Boundary-Layer Meteorol* 113:81–109
- Kolmogorov AN (1941) The local structure of turbulence in incompressible viscous fluid for very large Reynolds number. *Dokl Akad Nauk SSSR* 30:299–304
- Lesieur M (1991) *Turbulence in fluids*. Kluwer Academic Publishers, Dordrecht, The Netherlands, 412 pp
- Majda A, Kramer P (1999) Simplified models for turbulent diffusion: Theory, numerical modelling, and physical phenomena. *Phys Reports* 314:237–574

- Monin A, Yaglom A (1975) *Statistical fluid mechanics, Vol. II*. MIT Press, Cambridge, MA, 874 pp
- Panchev S (1971) *Random functions and turbulence*. Pergamon Press, New York, 444 pp
- Poggi D, Porporato A, Ridolfi L (2002) An experimental contribution to near-wall measurements by means of a special laser Doppler anemometry technique'. *Exp Fluids* 32:366–375
- Poggi D, Katul G, Albertson J (2004a) Momentum transfer and turbulent kinetic energy budgets within a dense model canopy. *Boundary-Layer Meteorol* 111(3):589–614
- Poggi D, Katul G, Albertson J (2004b) A note on the contribution of dispersive fluxes to momentum transfer within canopies. *Boundary-Layer Meteorol* 111(3):615–621
- Poggi D, Porporato A, Ridolfi L, Katul G, Albertson J (2004c) The effect of vegetation density on canopy sublayer turbulence. *Boundary-Layer Meteorol* 111(3):565–587
- Poggi D, Porporato A, Ridolfi L, Katul G, Albertson J (2004d) Interaction between large and small scales in the canopy sublayer. *Geophys Res Lett* 31(5):L05102
- Poggi D, Katul G, Albertson J (2006) Scalar dispersion within a model canopy: Measurements and three-dimensional Lagrangian models *Adv. Water Res* 29:326–335
- Shraiman B, Siggia E (2000) Scalar turbulence. *Nature* 405:639–646
- Siqueira M, Katul G, Lai C (2002) Quantifying net ecosystem exchange by multilevel ecophysiological and turbulent transport models. *Adv Water Res* 25:1357–1366
- Smagorinski J (1993) Some historical remarks on the use of non-linear viscosities: in large eddy simulation of complex engineering and geophysical flows. Cambridge University Press, Cambridge, UK, pp 4–36
- Tennekes H, Lumley J (1972) *A first course in turbulence*. MIT Press, Cambridge, MA, pp 49–80
- Warhaft Z (2000) Passive scalars in turbulent flows. *Ann Rev Fluid Mech* 32:203–240
- Wilson J (1988) A second order closure model for flow through vegetation. *Boundary-Layer Meteorol* 42:371–392